

Nonlinear Terahertz Metamaterials via Field-Enhanced Carrier Dynamics in GaAs

Kebin Fan,¹ Harold Y. Hwang,² Mengkun Liu,³ Andrew C. Strikwerda,³ Aaron Sternbach,³ Jingdi Zhang,³
Xiaoguang Zhao,¹ Xin Zhang,¹ Keith A. Nelson,² and Richard D. Averitt³

¹*Department of Mechanical Engineering, Boston University, 110 Cummington Street, Boston, Massachusetts 02215, USA*

²*Department of Chemistry, Massachusetts Institute of Technology, Cambridge, Massachusetts 02139, USA*

³*Department of Physics, Boston University, 590 Commonwealth Avenue, Boston, Massachusetts 02215, USA*

(Received 7 August 2012; revised manuscript received 5 March 2013; published 21 May 2013)

We demonstrate nonlinear metamaterial split ring resonators (SRRs) on GaAs at terahertz frequencies. For SRRs on doped GaAs films, incident terahertz radiation with peak fields of ~ 20 – 160 kV/cm drives intervalley scattering. This reduces the carrier mobility and enhances the SRR LC response due to a conductivity decrease in the doped thin film. Above ~ 160 kV/cm, electric field enhancement within the SRR gaps leads to efficient impact ionization, increasing the carrier density and the conductivity which, in turn, suppresses the SRR resonance. We demonstrate an increase of up to 10 orders of magnitude in the carrier density in the SRR gaps on semi-insulating GaAs. Furthermore, we show that the effective permittivity can be swept from negative to positive values with an increasing terahertz field strength in the impact ionization regime, enabling new possibilities for nonlinear metamaterials.

DOI: [10.1103/PhysRevLett.110.217404](https://doi.org/10.1103/PhysRevLett.110.217404)

PACS numbers: 78.20.Ci, 42.65.-k, 72.20.-i, 78.67.Pt

Nonlinear metamaterials is a rapidly developing field of fundamental interest with significant technological implications spanning from microwave through the visible spectral ranges [1–7]. As with tunable and reconfigurable metamaterials [8,9], the combination of the metamaterial structure with the local environment is crucial. This is because significant nonlinearities result from local field enhancement within the active region of the subwavelength metamaterial elements which, in the case of split ring resonators, are the capacitive gaps. While the active volume of the enhanced gaps is small in comparison to the unit cell volume, the field enhancement can dominate volumetric effects leading to global nonlinearities enhanced by 2 to 4 orders of magnitude [5]. This, in turn, results in useful nonlinear effects at low incident fields.

Advances in nonlinear metamaterials coincide with the development of high-field terahertz sources capable of generating electric fields sufficient to induce significant nonlinearities in conventional matter [10–14]. For example, in doped GaAs, highly nonlinear effects such as velocity saturation and impact ionization have been observed [11,14] at peak electric fields of several hundred kV/cm. Further, with metamaterial-enhanced THz electric fields of ~ 1 MV/cm, an insulator-metal phase transition has been induced in vanadium dioxide, a prototypical correlated electron material [7].

In this Letter, we experimentally demonstrate a nonlinear response in metamaterial split ring resonators (SRRs) on n -type GaAs and semi-insulating (SI) GaAs at terahertz frequencies. The nonlinear response arises from THz electric field-induced carrier dynamics that increase or decrease the conductivity of the substrate upon which the SRR arrays are fabricated. This modifies the SRR electromagnetic response as a function of field strength.

For peak incident THz fields (E_{in}) from ~ 20 – 160 kV/cm, mobility saturation by intervalley scattering (IVS) dominates, leading (for doped GaAs) to a conductivity decrease with a corresponding increase in the metamaterial oscillator strength. In this regime, electric field enhancement within the SRR capacitive gaps does not significantly contribute to the nonlinearity. That is, IVS occurs uniformly across the film independent of the SRRs. For $E_{in} \geq 160$ kV/cm, field enhancement in the gaps enables efficient carrier generation via impact ionization (IMI) resulting in a decrease in the SRR oscillator strength. It is possible to sweep the effective permittivity from negative to positive values by increasing the incident field strength, enabling new possibilities for nonlinear metamaterials such as an intensity dependent effective refractive index. We also show that SRRs on semi-insulating GaAs exhibit a nonlinear response arising from an increase of the in-gap conductivity by several orders of magnitude.

To create nonlinear metamaterials, electric field resonant SRR arrays were fabricated by conventional microfabrication on GaAs. Figure 1(a) shows an SRR array on a $1.8\text{-}\mu\text{m}$ -thick doped ($1 \times 10^{16} \text{ cm}^{-3}$) GaAs film deposited on a SI-GaAs substrate using molecular-beam epitaxy. The 7 by 7 mm² array of SRRs consists of 200-nm -thick Au with a 10 nm Cr adhesion layer. A narrow gap ($g = 2.2 \mu\text{m}$) is important as the field enhancement scales as $1/g$ [15]. To characterize the linear electromagnetic response, electro-optic based terahertz time-domain (THz-TDS) spectroscopy was employed. To accurately measure the metamaterial transmission spectrum, a bare n -type GaAs substrate was used as a reference. Dividing the Fourier transform of the sample data by that of the reference data yields the transmission amplitude as a function of the frequency as shown in Fig. 1(b). The LC

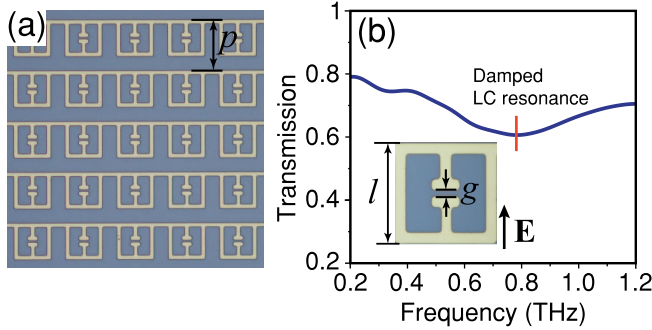


FIG. 1 (color online). (a) Image of the SRR array on n -type GaAs substrate. The period p is $50 \mu\text{m}$, the length of ring l is $36 \mu\text{m}$, and the gap g is $2.2 \mu\text{m}$. (b) Field transmission spectrum of the SRR array using THz time-domain spectroscopy on doped GaAs at low fields (i.e., in the linear response regime).

resonance is ~ 0.75 THz and is strongly damped, as expected, since carriers in the doped GaAs short the SRRs. The corresponding conductivity of doped GaAs is $\sim 7 (\Omega \text{cm})^{-1}$.

For the nonlinear transmission measurements, high-field THz experiments were performed using tilted-pulse-front THz generation in LiNbO_3 [16]. We obtained a peak THz field strength of approximately 400 kV/cm , with a 1-mm beam diameter at the focus. The field strength could be varied from 24 to 400 kV/cm using a pair of wire grid polarizers. The detailed experimental setup has been described elsewhere [10,17]. All experiments were performed at room temperature in a dry air environment at ambient pressure.

Figure 2(a) shows the experimentally measured transmission as a function of the frequency for various values of $E_{\text{in}} \leq 160 \text{ kV/cm}$. At 24 kV/cm the transmission response is similar to the low-field ($< 1 \text{ kV/cm}$) result shown in Fig. 1(b) where a weak LC resonance is observed. As the incident field is increased to 160 kV/cm , the LC resonance becomes quite pronounced, leading to a decrease in the resonant transmission (~ 0.73 THz) from 65% to about 30% . This suggests a decrease in the conductivity which, as discussed below, results from a decrease in the carrier mobility due to THz-induced IVS. The off-resonance transmission at low frequencies increases (e.g., at 0.4 THz from 80% to over 90%). This indicated a field-induced reduction in the conductivity of the entire n -type GaAs film similar to other tunable metamaterial responses [18,19] and consistent with the earlier observation in bulk GaAs [11]. Thus, for $24 \leq E_{\text{in}} \leq 160 \text{ kV/cm}$ the nonlinearity does not depend strongly on the in-gap field enhancement.

However above $\sim 160 \text{ kV/cm}$, the trend described above in the field-dependent transmission at the resonant frequency is reversed as shown in Fig. 2(b): the transmission increases with a further increase in E_{in} . This indicates a reversal of the underlying trend in conductivity, i.e., an increase in conductivity in the gaps as the field is

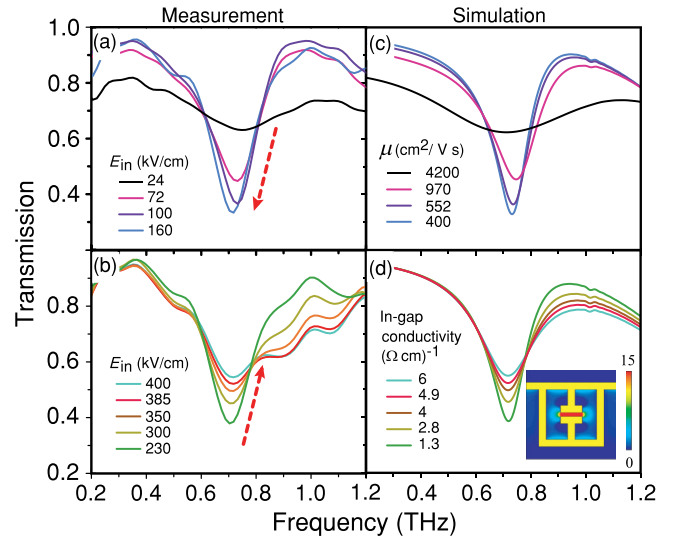


FIG. 2 (color online). (a) and (b) Experimental electric field transmission as a function of frequency for various incident peak electric fields. (c) Simulated transmission of the SRR array on doped GaAs film for different electron mobilities at a constant carrier density of $1 \times 10^{16} \text{ cm}^{-3}$. In these simulations the mobility of the carriers throughout the film is changed. μ is the electron mobility. (d) Simulated transmission on doped GaAs for various in-gap conductivities. In these simulations the mobility is constant and the carrier density is modified according to IMI simulations. The inset in (d) shows the simulated on-resonance field enhancement, highlighting that the largest enhancement occurs within the SRR gaps.

increased above 160 kV/cm . Notably, the off-resonance transmission at lower frequencies (< 0.5 THz) remains almost unchanged which implies a local conductivity increase solely in the capacitive gaps of the resonators. We ascribe this response to THz field-induced impact ionization.

To better understand how THz field-driven nonequilibrium carrier transport determines the nonlinear metamaterial response, we consider, in turn, IVS and IMI. For $24 \leq E_{\text{in}} \leq 160 \text{ kV/cm}$, electrons in the conduction band (Γ valley) are accelerated and acquire energy on the order of 1 eV , sufficient for scattering into satellite valleys. Since the mobility in the side valleys is approximately 1 order of magnitude smaller than in the Γ valley [20,21], IVS leads to a significant conductivity decrease in the n -type GaAs film. Independent of the SRR array, for doped substrates IVS results in photoinduced transparency [11,22,23] and accounts for the off-resonance transmission increase that is observed in Fig. 2(a). Of course, for the SRR arrays, this same process decreases the in-gap conductivity, resulting in an enhanced LC resonance.

IVS-induced enhancement of the metamaterial electromagnetic response was simulated using the commercial software package, CST Microwave Studio. The n -type GaAs film was modeled utilizing a frequency dependent Drude response. We assume that the average mobility

varies by changing the relative fraction of electrons in the Γ and L valleys and that at 160 kV/cm all of the conduction electrons are scattered to the L valley. Additionally, for fields ≤ 160 kV/cm, we neglect IMI. That is, the carrier concentration is held constant at the doping value (1×10^{16} cm $^{-3}$). The results of this mobility averaging procedure (applied to the entire film) determine the film conductivity used in the electromagnetic simulations. The results are shown in Fig. 2(c) and show good agreement with the experimental data in Fig. 2(a). Comparing these plots reveals that, for an incident field of 24 kV/cm, a mobility of 4200 cm 2 /Vs (close to the reported value [24]) yields good agreement. If the majority of conduction electrons were scattered to the L valley, a mobility of 400 cm 2 /Vs would result. The agreement between experiment and simulation suggests that at 160 kV/cm this a reasonable approximation.

Above 160 kV/cm, IMI becomes increasingly important. This is because the SRR resonance is strengthened from the IVS-induced conductivity decrease. At 160 kV/cm, simulations indicate in-gap electric field enhancement by a factor of ~ 15 on resonance, corresponding to an overall peak electric field enhancement of ~ 4 in the time domain. This is in good agreement with previously reported values [15]. Thus, with an incident field strength of 160 kV/cm, the in-gap field is estimated to be ~ 0.64 MV/cm, which is sufficient for IMI in which THz-accelerated conduction band electrons collide with valence band electrons to result in carrier generation (in the L valley) [13,14]. As a simple estimate, the motion of electrons under an external field is given as

$$\frac{d\langle v(t) \rangle}{dt} = \frac{eE(t)}{m_e} - \frac{\langle v(t) \rangle}{\tau(E)}, \quad (1)$$

where $\langle v(t) \rangle$ is the average electron velocity, $E(t)$ is the THz field, m_e is the effective electron mass, and τ is the relaxation time [25]. For n -type GaAs, IMI is favorable for electrons in the L valley when the kinetic energy of an electron reaches a threshold energy, $\mathcal{E}_{th} = 2.1$ eV [26]. Model calculations show that with an initial carrier density of 1×10^{16} /cm 3 , an incident field of 400 kV/cm (1.6 MV/cm in-gap field) can increase the carrier density up to $\sim 10^{17}$ /cm 3 . This process leads to an in-gap conductivity of ~ 6 (Ωcm) $^{-1}$. The calculated conductivity arising from IMI leads to reasonable agreement between experiment and simulation [Figs. 2(b) and 2(d)]. To obtain agreement between experiment and simulation at the highest fields, an average in-gap electron mobility of 240 cm 2 /Vs was used, which is consistent with increased carrier-carrier scattering at higher densities and in agreement with the lower end of the L valley mobility previously reported in optical carrier generation studies [20,21].

In contrast to doped GaAs, semi-insulating GaAs (SI-GaAs, carrier density $\sim 1 \times 10^7$ /cm 3) with its low conductivity of 1×10^{-8} (Ωcm) $^{-1}$ yields a distinct SRR resonance and THz field enhancement even at low incident

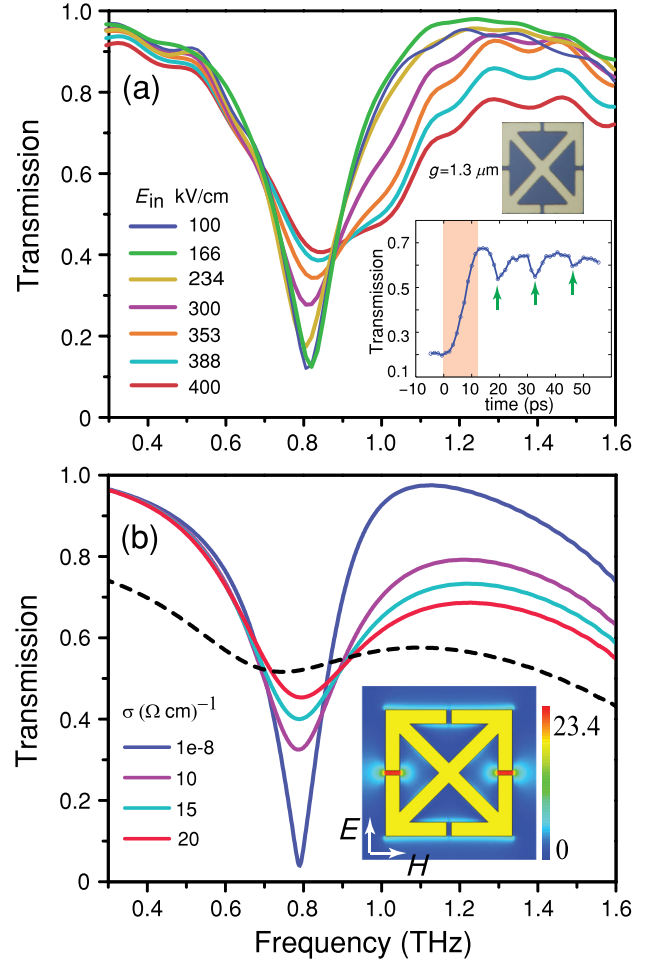


FIG. 3 (color online). (a) Experimental electric field transmission as a function of the frequency for various incident peak electric fields for SRRs on SI-GaAs. The top inset shows an image of the fabricated metamaterial unit cell with a gap size of 1.3 μm . The bottom inset shows the long-time dynamics from time-resolved THz-pump/THz-probe measurements of the 0.8 THz metamaterial resonance. The red region is where IMI preferentially occurs. The transmission dips noted by the green arrows are due to carrier mobility saturation from etalon reflections of the THz-pump field in the substrate. (b) Simulated transmission for SRRs on SI-GaAs as a function of frequency for various in-gap conductivities. The dashed curve is the predicted response if the entire lateral area of the GaAs substrate (to a depth of 0.5 μm) has a conductivity of 20 (Ωcm) $^{-1}$. This clearly disagrees with experiments suggesting that the carrier multiplication occurs only in the capacitive gaps of the SRRs. The inset shows the simulated on-resonance field enhancement.

field levels. The inset of Fig. 3 shows the SRR unit cell used to fabricate arrays on SI-GaAs. The size and period of the SRR resonators are the same as the resonators on the doped GaAs, thereby maintaining the resonance roughly at the same frequency. A smaller SRR gap (1.3 μm) was used to increase the field enhancement given the difficulty in initiating IMI on SI-GaAs due to the small initial carrier density. At our free-space THz field

strengths, IMI is ineffective as a carrier generation mechanism in SI-GaAs. However, with the additional field enhancement available from SRRs, we observed a nonlinear response on SI-GaAs that we attribute mainly to IMI.

Figure 3(a) shows the experimentally measured transmission of metamaterials as a function of the frequency for various values of E_{in} . At the lowest field (100 kV/cm), the response is still in the linear regime with a characteristic dip in the transmission at the LC resonance frequency. As the incident field increases, the metamaterial transmission increases and broadens with negligible change at lower frequencies. We note that even at the highest incident fields ($E_{in} = 400$ kV/cm), no nonlinear transmission changes were detected on bare SI-GaAs. Similar to the nonlinear high-field results (> 160 kV/cm) on n -type GaAs, the results of Fig. 3(a) suggest a large increase in the in-gap conductivity, indicating a carrier density increase via IMI.

Further evidence for carrier generation by IMI is provided by THz-pump/THz-probe measurements of the long-time dynamics of the 0.8 THz metamaterial resonance as shown in the bottom inset of Fig. 3(a). The transmission at the 0.8 THz resonance increases from 20% to 70% in the IMI regime (red region) and persists with little decay over the measurement time window. This persistent change in transmission is consistent with carrier generation in GaAs, where the electron-hole recombination time is much longer than the picosecond time scale of the measurements. We note that the change in transmission at the 0.8 THz resonance is much larger in the dynamic measurement than in the steady state nonlinear transmission measurement because the IMI process continues even after the THz-pump field has left the sample. There are also three dips (noted by green arrows in the figure) in the transmission at 0.8 THz due to carrier mobility saturation of the generated carriers in the capacitive gaps due to etalon reflections of the THz-pump field in the SI-GaAs substrate [11,27].

Electromagnetic simulations were performed by changing the conductivity of the GaAs in the horizontal gaps as shown in the inset of Fig. 3(b). The plot shows the transmission change upon increasing the in-gap conductivity from $10^{-8} (\Omega\text{cm})^{-1}$ to $20 (\Omega\text{cm})^{-1}$. The simulations show a trend that is markedly similar to the experimental results. The inset of Fig. 3(b) shows the field within the gaps is enhanced by over 20 times on resonance corresponding to a peak time-domain field enhancement factor of 7. Impact ionization calculations show that with an initial carrier density of $1 \times 10^{17}/\text{cm}^3$, an in-gap field of 2.8 MV/cm (corresponding to our largest incident field, $E_{in} = 400$ kV/cm) can increase the carrier density by more than 10 orders of magnitude up to $\sim 10^{18}/\text{cm}^3$. Although we attribute the carrier multiplication primarily to IMI, Zener tunneling cannot, *a priori*, be discounted. Tunneling calculations [28] show that with an in-gap peak field of 2.8 MV/cm, Zener tunneling can generate a free carrier density of $\sim 10^{17}/\text{cm}^3$, which is one order of

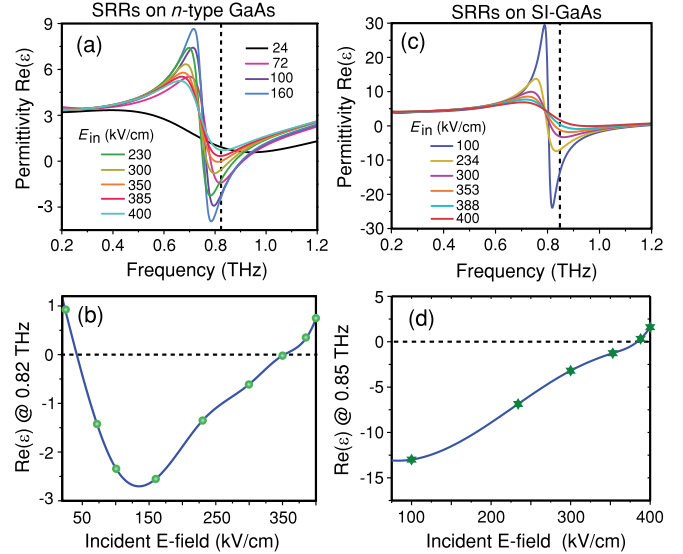


FIG. 4 (color online). (a) Effective real permittivity $\epsilon_{re}(\omega)$ for SRRs on doped GaAs for various incident electric fields. (b) $\epsilon_{re}(\omega)$ as a function of incident peak electric field strength at 0.82 THz for SRRs on doped GaAs. (c) $\epsilon_{re}(\omega)$ for SRRs on SI-GaAs for various incident electric fields. (d) $\epsilon_{re}(\omega)$ as a function of incident peak electric field strength at 0.85 THz for SRRs on SI-GaAs.

magnitude smaller than that reached by IMI. This indicates that carrier generation may involve both processes.

One consequence of embedding metallic resonators into nonlinear dielectrics is the enhancement of the effective nonlinearity by 2 to 4 orders of magnitude (in comparison to the bare nonlinear material) because of the in-gap field enhancement [29]. For our metamaterials, the nonlinearity results in a change of the oscillator strength of the LC resonance. Because of dispersion, this leads to changes in the effective permittivity and refractive index at frequencies away from resonance. The effective real permittivity (ϵ_{re}) is shown as a function of frequency for various incident electric fields for SRRs on n -type GaAs [Fig. 4(a)] and SI-GaAs [Fig. 4(c)]. These plots were obtained by performing parameter extraction (for a cubic unit cell) using the full-wave simulations [30–32] of Figs. 2(c), 2(d), and 3(b) and subsequently mapping the in-gap conductivity to the corresponding incident peak electric field required to achieve that conductivity. It is clear that the field dependence of ϵ_{re} is different for the two cases. For the SRRs on n -type GaAs, the off-resonance ϵ_{re} at 0.82 THz changes from positive to negative owing to IVS in the doped thin film. Above 160 kV/cm, ϵ_{re} increases from negative to positive values due to the onset of IMI [Fig. 4(b)]. For SRRs on SI-GaAs, IMI increases ϵ_{re} monotonically from negative to positive values at 0.85 THz [Fig. 4(d)].

We have demonstrated that metamaterials enable strongly enhanced nonlinearities at terahertz frequencies. The present study illustrates strong THz-induced changes in the carrier mobility and density, yielding conductivity

changes up to 10 orders of magnitude and large changes in THz transmission. As our proof-of-principle results demonstrate, it will be possible to create a host of nonlinear THz metamaterials which includes, as but one example, nonlinear absorbers for saturable absorber or optical limiting applications.

The authors acknowledge support from ONR Grant No. N00014-09-1-1103, AFOSR Grant No. FA9550-09-1-0708, and from DTRA C&B Technologies Directorate administered through a subcontract from ARL. We would also like to thank Grace Metcalfe and Mike Wraback of ARL for providing the MBE grown n -type GaAs.

-
- [1] A. A. Zharov, I. V. Shadrivov, and Y. S. Kivshar, *Phys. Rev. Lett.* **91**, 037401 (2003).
- [2] M. W. Klein, M. Wegener, N. Feth, and S. Linden, *Opt. Express* **15**, 5238 (2007).
- [3] B. Wang, J. Zhou, Th. Koschny, and C. M. Soukoulis, *Opt. Express* **16**, 16 058 (2008).
- [4] A. Fang, T. Koschny, M. Wegener, and C. M. Soukoulis, *Phys. Rev. B* **79**, 241104 (2009).
- [5] E. Pourtrina, D. Huang, and D. R. Smith, *New J. Phys.* **12**, 093010 (2010).
- [6] A. Rose, D. Huang, and D. R. Smith, *Phys. Rev. Lett.* **107**, 063902 (2011).
- [7] M.-K. Liu *et al.*, *Nature (London)* **487**, 345 (2012).
- [8] H.-T. Chen, W. J. Padilla, J. M. O. Zide, A. C. Gossard, A. J. Taylor, and R. D. Averitt, *Nature (London)* **444**, 597 (2006).
- [9] H. Tao, A. C. Strikwerda, K. Fan, W. J. Padilla, X. Zhang, and R. D. Averitt, *Phys. Rev. Lett.* **103**, 147401 (2009).
- [10] M. C. Hoffmann, J. Hebling, H. Y. Hwang, K.-L. Yeh, and K. A. Nelson, *Phys. Rev. B* **79**, 161201 (2009).
- [11] J. Hebling, M. C. Hoffmann, H. Y. Hwang, K.-L. Yeh, and K. A. Nelson, *Phys. Rev. B* **81**, 035201 (2010).
- [12] I.-C. Ho, and X.-C. Zhang, *Appl. Phys. Lett.* **98**, 241908 (2011).
- [13] K. Tanaka, H. Hirori, and M. Nagai, *IEEE Trans. Tera. Sci. Tech.* **1**, 301 (2011).
- [14] H. Hirori, K. Shinokita, M. Shirai, S. Tani, Y. Kadoya, and K. Tanaka, *Nat. Commun.* **2**, 594 (2011).
- [15] C. A. Werley, K. Fan, A. C. Strikwerda, S. M. Teo, X. Zhang, R. D. Averitt, and K. A. Nelson, *Opt. Express* **20**, 8551 (2012).
- [16] K.-L. Yeh, M. C. Hoffmann, J. Hebling, and K. A. Nelson, *Appl. Phys. Lett.* **90**, 171121 (2007).
- [17] J. Hebling, K.-L. Yeh, M. C. Hoffmann, and K. A. Nelson, *IEEE J. Quantum Electron.* **14**, 345 (2008).
- [18] T. Driscoll *et al.*, *Appl. Phys. Lett.* **93**, 024101 (2008).
- [19] N.-H. Shen, M. Massaouti, M. Gokkavas, J.-M. Manceau, E. Ozbay, M. Kafesaki, T. Koschny, S. Tzortzakis, and C. M. Soukoulis, *Phys. Rev. Lett.* **106**, 037403 (2011).
- [20] J. T. Darrow, X.-C. Zhang, D. H. Auston, and J. D. Morse, *IEEE J. Quantum Electron.* **28**, 1607 (1992).
- [21] M. C. Nuss, D. H. Auston, and F. Capasso, *Phys. Rev. Lett.* **58**, 2355 (1987).
- [22] F. H. Su *et al.*, *Opt. Express* **17**, 9620 (2009).
- [23] S. J. Allen, C. L. Allyn, H. M. Cox, F. DeRosa, and G. E. Mahoney, *Appl. Phys. Lett.* **42**, 96 (1983).
- [24] N. Katzenellenbogen and D. Grischkowsky, *Appl. Phys. Lett.* **61**, 840 (1992).
- [25] W. Kuehn, P. Gaal, K. Reimann, M. Woerner, T. Elsaesser, and R. Hey, *Phys. Rev. Lett.* **104**, 146602 (2010).
- [26] C. L. Anderson and C. R. Crowell, *Phys. Rev. B* **5**, 2267 (1972).
- [27] M. C. Beard, G. M. Turner, and C. A. Schmuttenmaer, *Phys. Rev. B* **62**, 15 764 (2000).
- [28] P. Rodin, U. Ebert, W. Hundsdorfer, and I. Grekhov, *J. Appl. Phys.* **92**, 958 (2002).
- [29] A. Rose, S. Larouche, and D. R. Smith, *Phys. Rev. A* **84**, 053805 (2011).
- [30] R. Smith, S. Schultz, P. Markoš, and C. M. Soukoulis, *Phys. Rev. B* **65**, 195104 (2002).
- [31] D. R. Smith, D. C. Vier, Th. Koschny, and C. M. Soukoulis, *Phys. Rev. E* **71**, 036617 (2005).
- [32] H. Tao, A. C. Strikwerda, K. Fan, C. M. Bingham, W. J. Padilla, X. Zhang, and R. D. Averitt, *J. Phys. D* **41**, 232004 (2008).